ResearchGate

See discussions, stats, and author profiles for this publication at: https://www.researchgate.net/publication/44650656

In Situ Reactivity and TOF-SIMS Analysis of Surfaces Prepared by Soft and Reactive Landing of Mass-Selected Ions

ARTICLE *in* ANALYTICAL CHEMISTRY · JULY 2010

Impact Factor: 5.64 · DOI: 10.1021/ac100734g · Source: PubMed

READS

9

3 AUTHORS, INCLUDING:

Grant Johnson

Pacific Northwest National Laboratory

44 PUBLICATIONS **987** CITATIONS

SEE PROFILE

Julia Laskin

Pacific Northwest National Laboratory

209 PUBLICATIONS **4,787** CITATIONS

SEE PROFILE

Available from: Grant Johnson
Retrieved on: 29 January 2016

Anal. Chem. **2010,** *82,* 5718–5727

In Situ Reactivity and TOF-SIMS Analysis of Surfaces Prepared by Soft and Reactive Landing of Mass-Selected Ions

Grant E. Johnson,* Michael Lysonski,† and Julia Laskin*

Chemical and Materials Sciences Division, Pacific Northwest National Laboratory, P.O. Box 999, MSIN K8-88, Richland, Washington 99352

An instrument has been designed and constructed that enables in situ reactivity and time-of-flight secondary ion mass spectrometry (TOF-SIMS) analysis of surfaces prepared or modified through soft and reactive landing of mass-selected polyatomic cations and anions. The apparatus employs an electrospray ion source coupled to a high transmission electrodynamic ion funnel, two focusing collision quadrupoles, a large 19 mm diameter quadrupole mass filter, and a quadrupole bender that deflects the ion beam, thereby preventing neutral contaminants from impinging on the deposition surface. The ion soft landing apparatus is coupled to a commercial TOF-SIMS instrument permitting the introduction of surfaces into vacuum and SIMS analysis before and after ion deposition without breaking vacuum. To facilitate a comparison of the current TOF-SIMS instrument with the in situ Fourier transform ion cyclotron resonance (FTICR-SIMS) deposition apparatus constructed previously, dications of the cyclic peptide Gramicidin S (GS) and the photoactive organonometallic complex ruthenium tris-bipyridine ($Ru(bpy)_3$) were soft-landed onto fluorinated self-assembled monolayer (FSAM) on gold surfaces. In both cases, similarities and differences were observed in the secondary ion mass spectra, with the TOF-SIMS results, in general, characterized by greater sensitivity, larger dynamic range, less fragmentation, and fewer in-plume reactions than the corresponding FTICR-SIMS spectra. The charge reduction kinetics of both the doubly and singly protonated GS cations on the FSAM surface were also examined as was the influence of the primary gallium ion (Ga^+) flux on the efficiency of these processes. In addition, we demonstrate that the new instrument enables detailed studies of the reactivity of catalytically active species immobilized by soft and reactive landing toward gaseous reagents.

The deposition of mass selected ions onto surfaces has become a topic of considerable recent interest due to its promising potential as a technique for the highly controlled preparation of materials. Recent efforts, for example, have indicated possible future applications in production of peptide and protein microarrays for use in high throughput screening,[1−7] protein separation, and conformational enrichment of peptides,[8,9] chiral enrichment of organic compounds,[10] redox protein characterization,[11−13] thin film production,[14,15] processing of graphene,[16] and the preparation of catalysts through deposition of clusters and organometallic complexes.[17−23] The idea of modifying surfaces through the soft landing of polyatomic ions was first proposed by Cooks and co-

* To whom correspondence should be addressed. G. E. Johnson, J. Laskin, Pacific Northwest National Laboratory, Richland, WA 99352. E-mail: Grant.Johnson@pnl.gov, Julia.Laskin@pnl.gov.

† Undergraduate student from Carleton College, MN.

(1) Ouyang, Z.; Takats, Z.; Blake, T. A.; Gologan, B.; Guymon, A. J.; Wiseman, J. M.; Oliver, J. C.; Davisson, V. J.; Cooks, R. G. *Science* **2003**, *301*, 1351–1354.
(2) Blake, T. A.; Zheng, O. Y.; Wiseman, J. M.; Takats, Z.; Guymon, A. J.; Kothari, S.; Cooks, R. G. *Anal. Chem.* **2004**, *76*, 6293–6305.
(3) Wang, P.; Hadjar, O.; Laskin, J. *J. Am. Chem. Soc.* **2007**, *129*, 8682–8683.
(4) Wang, P.; Hadjar, O.; Gassman, P. L.; Laskin, J. *Phys. Chem. Chem. Phys.* **2008**, *10*, 1512–1522.
(5) Volny, M.; Elam, W. T.; Branca, A.; Ratner, B. D.; Turecek, F. *Anal. Chem.* **2005**, *77*, 4890–4896.
(6) Volny, M.; Elam, W. T.; Ratner, B. D.; Turecek, F. *Anal. Chem.* **2005**, *77*, 4846–4853.
(7) Volny, M.; Elam, W. T.; Ratner, B. D.; Turecek, F. *J. Biomed. Mater. Res. B* **2007**, *80B*, 505–510.
(8) Gologan, B.; Takats, Z.; Alvarez, J.; Wiseman, J. M.; Talaty, N.; Ouyang, Z.; Cooks, R. G. *J. Am. Soc. Mass Spectrom.* **2004**, *15*, 1874–1884.
(9) Wang, P.; Laskin, J. *Angew. Chem., Int. Ed.* **2008**, *47*, 6678–6680.
(10) Nanita, S. C.; Takats, Z.; Cooks, R. G. *J. Am. Soc. Mass Spectrom.* **2004**, *15*, 1360–1365.
(11) Mazzei, F.; Favero, G.; Frasconi, M.; Tata, A.; Tuccitto, N.; Licciardello, A.; Pepi, F. *Anal. Chem.* **2008**, *80*, 5937–5944.
(12) Mazzei, F.; Favero, G.; Frasconi, M.; Tata, A.; Pepi, F. *Chem.—Eur. J.* **2009**, *15*, 7359–7367.
(13) Pepi, F.; Ricci, A.; Tata, A.; Favero, G.; Frasconi, M.; Noci, S. D.; Mazzei, F. *Chem. Commun.* **2007**, 3494–3496.
(14) Rauschenbach, S.; Vogelgesang, R.; Malinowski, N.; Gerlach, J. W.; Benyoucef, M.; Costantini, G.; Deng, Z. T.; Thontasen, N.; Kern, K. *Acs Nano* **2009**, *3*, 2901–2910.
(15) Saf, R.; Goriup, M.; Steindl, T.; Hamedinger, T. E.; Sandholzer, D.; Hayn, G. *Nat. Mater.* **2004**, *3*, 323–329.
(16) Rader, H. J.; Rouhanipour, A.; Talarico, A. M.; Palermo, V.; Samori, P.; Mullen, K. *Nat. Mater.* **2006**, *5*, 276–280.
(17) Heiz, U.; Schneider, W. D. *Crit. Rev. Solid State* **2001**, *26*, 251–290.
(18) Kaden, W. E.; Wu, T. P.; Kunkel, W. A.; Anderson, S. L. *Science* **2009**, *326*, 826–829.
(19) Bottcher, A.; Weis, P.; Bihlmeier, A.; Kappes, M. M. *Phys. Chem. Chem. Phys.* **2004**, *6*, 5213–5217.
(20) Vajda, S.; Winans, R. E.; Elam, J. W.; Lee, B. D.; Pellin, M. J.; Seifert, S.; Tikhonov, G. Y.; Tomczyk, N. A. *Top. Catal.* **2006**, *39*, 161–166.
(21) Winans, R. E.; Vajda, S.; Ballentine, G. E.; Elam, J. W.; Lee, B. D.; Pelline, M. J.; Seifert, S.; Tikhonov, G. Y.; Tomczyk, N. A. *Top. Catal.* **2006**, *39*, 145–149.
(22) Rauschenbach, S.; Stadler, F. L.; Lunedei, E.; Malinowski, N.; Koltsov, S.; Costantini, G.; Kern, K. *Small* **2006**, *2*, 540–547.
(23) Judai, K.; Sera, K.; Amatsutsumi, S.; Yagi, K.; Yasuike, T.; Yabushita, S.; Nakajima, A.; Kaya, K. *Chem. Phys. Lett.* **2001**, *334*, 277–284.

10.1021/ac100734g © 2010 American Chemical Society
Published on Web 06/04/2010

workers in 1977,[24] and in the intervening years, a variety of instrumental approaches have been developed for the deposition of mass-selected species from the gas-phase.[25] Ions have been generated through electrospray ionization,[1−3,8−14] matrix-assisted laser desorption/ionization,[16] electron impact ionization,[19,26] pulsed arc discharge,[27] gas condensation,[28] magnetron sputtering,[29] and laser vaporization;[30] mass selection has been accomplished mainly using quadrupole mass filters,[26,31−33] magnetic deflection,[34,35] and linear ion traps.[36,37] With these techniques, the interaction of hyperthermal (<100 eV) ions with surfaces has been studied extensively in an effort to better understand the factors influencing the efficiency of soft and reactive landing and the competing processes of both reactive and unreactive scattering as well as surface-induced dissociation.[25,38−46]

A potentially promising application of ion soft and reactive landing is the preparation of monodisperse catalyst materials.[47] In the regime of small metal clusters, where properties do not scale linearly with size, it has been shown that the addition or removal of single atoms can have a pronounced influence on chemical reactivity.[48] This effect was elegantly demonstrated by Heiz and co-workers[49,50] for a model catalyst consisting of 8 atom gold clusters supported on MgO. A number of subsequent studies have also provided strong evidence of the size-dependent reactivity of deposited metal clusters.[18,51−55] Moreover, recent findings indicate that small clusters containing as few as 10 and 55 atoms[56,57] are responsible for the enhanced activity of industrial gold catalysts supported on iron oxide, suggesting that improved future catalysts will predominately incorporate extremely small clusters. Through ion deposition, it is possible to generate stable arrays of small size-selected clusters that do not diffuse and agglomerate on the surface.[58,59] This suggests that with proper development of the technique, soft and reactive landing of clusters and small nanoparticles onto chosen supports may result in the creation of highly active heterogeneous catalysts.

In a similar vein, organometallic complexes that are used as solution phase homogeneous catalysts may also be immobilized on surfaces through reactive landing. Tethering organometallic complexes to solid supports to form hybrid organic−inorganic interfaces is currently an active area of research.[60] The key objective is to maintain the high selectivity of the solution phase complex while facilitating an easier separation of catalyst from products.[61] Through selection of an appropriate surface, it is possible to preserve or enhance the ligand environment surrounding the metal center while effecting strong immobilization.[62] Self-assembled monolayers (SAMs) on gold, which may be terminated with a variety of functionalities, are ideal templates to test the feasibility of immobilizing organometallics through reactive landing. Moreover, ionization techniques such as atmospheric pressure thermal desorption ionization (APTDI) have been shown to be capable of generating mixed metal inorganic complexes that are not easily accessible in the solution phase,[63] suggesting that soft landing may provide a route to unique inorganic compounds on surfaces. The instrument described in this publication has been constructed to examine the feasibility of preparing both heterogeneous and immobilized homogeneous catalysts through the soft and reactive landing of mass-selected polyatomic ions onto inorganic and self-assembled monolayer surfaces.

Characterization of the chemical and physical properties of surfaces following soft and reactive landing of ions is critical to the

(24) Franchetti, V.; Solka, B. H.; Baitinger, W. E.; Amy, J. W.; Cooks, R. G. *Int. J. Mass Spectrom. Ion Processes* **1977**, *23*, 29–35.
(25) Grill, V.; Shen, J.; Evans, C.; Cooks, R. G. *Rev. Sci. Instrum.* **2001**, *72*, 3149–3179.
(26) Miller, S. A.; Luo, H.; Pachuta, S. J.; Cooks, R. G. *Science* **1997**, *275*, 1447–1450.
(27) Siekmann, H. R.; Luder, C.; Faehrmann, J.; Lutz, H. O.; Meiwesbroer, K. H. *Z. Phys. D: Atom Mol. Cl.* **1991**, *20*, 417–420.
(28) Goldby, I. M.; vonIssendorff, B.; Kuipers, L.; Palmer, R. E. *Rev. Sci. Instrum.* **1997**, *68*, 3327–3334.
(29) Pratontep, S.; Carroll, S. J.; Xirouchaki, C.; Streun, M.; Palmer, R. E. *Rev. Sci. Instrum.* **2005**, *76*, 045103.
(30) Milani, P.; Deheer, W. A. *Rev. Sci. Instrum.* **1990**, *61*, 1835–1838.
(31) Alvarez, J.; Cooks, R. G.; Barlow, S. E.; Gaspar, D. J.; Futrell, J. H.; Laskin, *J. Anal. Chem.* **2005**, *77*, 3452–3460.
(32) Hadjar, O.; Wang, P.; Futrell, J. H.; Dessiaterik, Y.; Zhu, Z. H.; Cowin, J. P.; Iedema, M. J.; Laskin, *J. Anal. Chem.* **2007**, *79*, 6566–6574.
(33) Song, Q. Y.; Smith, S. A.; Gao, L.; Xu, W.; Volny, M.; Zheng, O. Y.; Cooks, R. G. *Anal. Chem.* **2009**, *81*, 1833–1840.
(34) Mayer, P. S.; Turecek, F.; Lee, H. N.; Scheidemann, A. A.; Olney, T. N.; Schumacher, F.; Strop, P.; Smrcina, M.; Patek, M.; Schirlin, D. *Anal. Chem.* **2005**, *77*, 4378–4384.
(35) Kemper, P.; Kolmakov, A.; Tong, X.; Lilach, Y.; Benz, L.; Manard, M.; Metiu, H.; Buratto, S. K.; Bowers, M. T. *Int. J. Mass Spectrom.* **2006**, *254*, 202–209.
(36) Nie, Z. X.; Li, G. T.; Goodwin, M. P.; Gao, L.; Cyriac, J.; Cooks, R. G. *J. Am. Soc. Mass Spectrom.* **2009**, *20*, 949–956.
(37) Peng, W. P.; Goodwin, M. P.; Nie, Z. X.; Volny, M.; Zheng, O. Y.; Cooks, R. G. *Anal. Chem.* **2008**, *80*, 6640–6649.
(38) Gologan, B.; Green, J. R.; Alvarez, J.; Laskin, J.; Cooks, R. G. *Phys. Chem. Chem. Phys.* **2005**, *7*, 1490–1500.
(39) Laskin, J.; Futrell, J. H. *Mass Spectrom. Rev.* **2003**, *22*, 158–181.
(40) Laskin, J.; Futrell, J. H. *Mass Spectrom. Rev.* **2005**, *24*, 135–167.
(41) Laskin, J.; Wang, P.; Hadjar, O. *Phys. Chem. Chem. Phys.* **2008**, *10*, 1079–1090.
(42) Vekey, K.; Somogyi, A.; Wysocki, V. H. *J. Mass Spectrom.* **1995**, *30*, 212–217.
(43) Wysocki, V. H.; Jones, C. M.; Galhena, A. S.; Blackwell, A. E. *J. Am. Soc. Mass Spectrom.* **2008**, *19*, 903–913.
(44) Wysocki, V. H.; Joyce, K. E.; Jones, C. M.; Beardsley, R. L. *J. Am. Soc. Mass Spectrom.* **2008**, *19*, 190–208.
(45) Jacobs, D. C. *Annu. Rev. Phys. Chem.* **2002**, *53*, 379–407.
(46) Cooks, R. G.; Ast, T.; Pradeep, T.; Wysocki, V. *Acc. Chem. Res.* **1994**, *27*, 316–323.
(47) Abbet, S.; Judai, K.; Klinger, L.; Heiz, U. *Pure Appl. Chem.* **2002**, *74*, 1527–1535.
(48) Bernhardt, T. M. *Int. J. Mass Spectrom.* **2005**, *243*, 1–29.
(49) Sanchez, A.; Abbet, S.; Heiz, U.; Schneider, W. D.; Hakkinen, H.; Barnett, R. N.; Landman, U. *J. Phys. Chem. A* **1999**, *103*, 9573–9578.
(50) Yoon, B.; Hakkinen, H.; Landman, U.; Worz, A. S.; Antonietti, J. M.; Abbet, S.; Judai, K.; Heiz, U. *Science* **2005**, *307*, 403–407.
(51) Worz, A. S.; Judai, K.; Abbet, S.; Heiz, U. *J. Am. Chem. Soc.* **2003**, *125*, 7964–7970.
(52) Rottgen, M. A.; Abbet, S.; Judai, K.; Antonietti, J. M.; Worz, A. S.; Arenz, M.; Henry, C. R.; Heiz, U. *J. Am. Chem. Soc.* **2007**, *129*, 9635–9639.
(53) Lee, S. S.; Fan, C. Y.; Wu, T. P.; Anderson, S. L. *J. Am. Chem. Soc.* **2004**, *126*, 5682–5683.
(54) Lee, S.; Fan, C. Y.; Wu, T. P.; Anderson, S. L. *J. Phys. Chem. B* **2005**, *109*, 381–388.
(55) Wu, T. P.; Kaden, W. E.; Kunkel, W. A.; Anderson, S. L. *Surf. Sci.* **2009**, *603*, 2764–2770.
(56) Herzing, A. A.; Kiely, C. J.; Carley, A. F.; Landon, P.; Hutchings, G. J. *Science* **2008**, *321*, 1331–1335.
(57) Turner, M.; Golovko, V. B.; Vaughan, O. P. H.; Abdulkin, P.; Berenguer-Murcia, A.; Tikhov, M. S.; Johnson, B. F. G.; Lambert, R. M. *Nature* **2008**, *454*, 981–983.
(58) Palmer, R. E.; Pratontep, S.; Boyen, H. G. *Nat. Mater.* **2003**, *2*, 443–448.
(59) Carroll, S. J.; Pratontep, S.; Streun, M.; Palmer, R. E.; Hobday, S.; Smith, R. *J. Chem. Phys.* **2000**, *113*, 7723–7727.
(60) Coperet, C.; Chabanas, M.; Saint-Arroman, R. P.; Basset, J. M. *Angew. Chem., Int. Ed.* **2003**, *42*, 156–181.
(61) Baker, R. T.; Kobayashi, S.; Leitner, W. *Adv. Synth. Catal.* **2006**, *348*, 1337–1340.
(62) Notestein, J. M.; Katz, A. *Chem.—Eur. J.* **2006**, *12*, 3954–3965.
(63) Peng, W. P.; Goodwin, M. P.; Chen, H.; Cooks, R. G.; Wilker, J. *Rapid Commun. Mass Spectrom.* **2008**, *22*, 3540–3548.

development of preparative mass spectrometry as a technique for the highly controlled production of materials. To date, a variety of techniques have been employed for this purpose including secondary ion mass spectrometry,[31,36] laser desorption ionization,[8] temperature programmed desorption and reaction (TPD),[64−68] pulsed molecular beam reaction,[69] cavity ringdown spectroscopy,[70−72] infrared spectroscopy (IR),[4,73,74] surface enhanced Raman spectroscopy (SERS),[75] X-ray photoelectron spectroscopy (XPS),[18,76−78] scanning tunneling microscopy (STM),[79,80] and atomic force microscopy (AFM).[22] In order to accurately investigate the true state of a surface prepared or modified by ion deposition it is crucial that the analysis be conducted in situ without exposure of the substrate to laboratory air. Previous in situ studies have enabled detailed understanding of phenomena such as the charge reduction and desorption of ions on surfaces, the kinetics of reactive landing, and the influence of size on the catalytic activity of deposited clusters.[18] By way of example, in our laboratory, we have studied the charge reduction kinetics of protonated peptides on FSAM,[31,81−83] HSAM,[81,82] and COOH-SAM[82] surfaces. The majority of these studies were conducted using an ion deposition apparatus coupled to a Fourier transform ion cyclotron resonance secondary ion mass spectrometer (FTICR-SIMS) that enabled in situ analysis of surfaces both during and after soft landing.[31] Ex situ analysis was also conducted by TOF-SIMS and infrared reflection absorption spectroscopy (IRRAS)[32] providing important insight into the secondary structure of complex ions immobilized by the soft landing and reactive landing processes. For example, it was demonstrated, using IRRAS that soft and reactive landing may be utilized for preparation of conformationally selected peptide arrays[9] and for efficient reactive immobilization of peptides onto *N*-hydroxysuccinimidyl ester functionalized SAMs.[3,4] More recently, an instrument has been constructed that allows in situ characterization of the soft and reactive landing of ions onto SAMs using IRRAS.[74] This spectroscopic technique enables bond formation processes as well as conformational changes to be observed in real time both during and after deposition. In the future, we aim to use in situ TOF-SIMS characterization to identify intermediates formed by the deposition of catalytically active organometallic complexes, to understand how exposure of substrates to ambient conditions influences their properties, and to determine the reactivity of deposited species by exposing them to controlled pressures of reactant gases. TOF-SIMS is a particularly sensitive technique for the analysis of surfaces, even in comparison to FTICR-SIMS, which is important for detecting low quantities of reactive intermediates produced during catalytic reactions. Moreover, due to its imaging capabilities, the TOF-SIMS technique will enable the analysis of patterned surfaces produced though ion soft and reactive landing.

Herein we report the design and implementation of an instrument for the in situ reactivity and TOF-SIMS analysis of surfaces produced through soft and reactive landing of mass selected ions. This is achieved by coupling a custom built ion deposition apparatus to a commercial TOF-SIMS instrument. We compare the results obtained for the deposition of doubly protonated Gramicidin $[GS + 2H]^{2+}$ and the organometallic dication $Ru(bpy)_3^{2+}$ onto FSAM with those obtained previously using FTICR-SIMS. It is shown that the TOF-SIMS technique is characterized by higher sensitivity, a larger overall dynamic range, less fragmentation and fewer in-plume reactions than FTICR-SIMS, which greatly simplifies SIMS spectra and facilitates identification of immobilized species. In addition, the utility of this instrument for kinetic studies is evaluated by examining the charge reduction kinetics of both doubly and singly protonated GS on the FSAM surface. The flux of the primary Ga^+ ion during the SIMS analysis is demonstrated to exhibit a pronounced influence on these processes. Finally, we provide an example of the immobilization of a catalytic organometallic complex on a SAM surface through reactive landing and demonstrate its reactivity toward gas-phase reagents.

EXPERIMENTAL SECTION

The apparatus constructed for soft and reactive landing of polyatomic ions onto surfaces is illustrated schematically in Figure 1 and described below.

Generation and Manipulation of Ion Beam. An electrospray ion source,[84] described in detail in a previous publication,[85] is used to generate gas-phase ions for subsequent mass-selection and deposition onto surfaces. Briefly, a syringe pump (model 100, KD Scientific, Inc., Holliston, MA) is used to propel a solution (typically in methanol or acetonitrile) through a 40 cm long, 190 μm outer diameter fused silica capillary that is biased between +2 to +3 kV for the generation of positive ions. Solution flow

(64) Harding, C.; Habibpour, V.; Kunz, S.; Farnbacher, A. N. S.; Heiz, U.; Yoon, B.; Landman, U. *J. Am. Chem. Soc.* **2009**, *131*, 538–548.
(65) Loffler, D.; Jester, S. S.; Weis, P.; Bottcher, A.; Kappes, M. M. *J. Chem. Phys.* **2006**, *124*, 054705.
(66) Nagaoka, S.; Matsumoto, T.; Okada, E.; Mitsui, M.; Nakajima, A. *J Phys Chem B* **2006**, *110*, 16008–16017.
(67) Mitsui, M.; Nagaoka, S.; Matsumoto, T.; Nakajima, A. *J Phys Chem B* **2006**, *110*, 2968–2971.
(68) Nagaoka, S.; Matsumoto, T.; Ikemoto, K.; Mitsui, M.; Nakajima, A. *J. Am. Chem. Soc.* **2007**, *129*, 1528–1529.
(69) Harding, C. J.; Kunz, S.; Habibpour, V.; Teslenko, V.; Arenz, M.; Heiz, U. *J. Catal.* **2008**, *255*, 234–240.
(70) Gilb, S.; Hartl, K.; Kartouzian, A.; Peter, J.; Heiz, U.; Boyen, H. G.; Ziemann, P. *Eur. Phys. J. D* **2007**, *45*, 501–506.
(71) Del Vitto, A.; Pacchioni, G.; Lim, K. H.; Rosch, N.; Antonietti, J. M.; Michalski, M.; Heiz, U.; Jones, H. *J. Phys. Chem. B* **2005**, *109*, 19876–19884.
(72) Kartouzian, A.; Thamer, M.; Soini, T.; Peter, J.; Pitschi, P.; Gilb, S.; Heiz, U. *J. Appl. Phys.* **2008**, *104*, 124313.
(73) Vanolli, F.; Heiz, U.; Schneider, W. D. *Chem. Phys. Lett.* **1997**, *277*, 527–531.
(74) Hu, Q. C.; Wang, P.; Gassman, P. L.; Laskin, *J. Anal. Chem.* **2009**, *81*, 7302–7308.
(75) Volny, M.; Sengupta, A.; Wilson, C. B.; Swanson, B. D.; Davis, E. J.; Turecek, F. *Anal. Chem.* **2007**, *79*, 4543–4551.
(76) Wijesundara, M. B. J.; Hanley, L.; Ni, B.; Sinnott, S. B. *Proc. Natl. Acad. Sci. U.S.A.* **2000**, *97*, 23–27.
(77) Wijesundara, M. B. J.; Ji, Y.; Ni, B.; Sinnott, S. B.; Hanley, L. *J. Appl. Phys.* **2000**, *88*, 5004–5016.
(78) Evans, C.; Wade, N.; Pepi, F.; Strossman, G.; Schuerlein, T.; Cooks, R. G. *Anal. Chem.* **2002**, *74*, 317–323.
(79) Messerli, S.; Schintke, S.; Morgenstern, K.; Sanchez, A.; Heiz, U.; Schneider, W. D. *Surf. Sci.* **2000**, *465*, 331–338.
(80) Kaiser, B.; Bernhardt, T. M.; Stegemann, B.; Opitz, J.; Rademann, K. *Phys. Rev. Lett.* **1999**, *83*, 2918–2921.
(81) Alvarez, J.; Futrell, J. H.; Laskin, J. *J. Phys. Chem. A* **2006**, *110*, 1678–1687.
(82) Laskin, J.; Wang, P.; Hadjar, O.; Futrell, J. H.; Alvarez, J.; Cooks, Z. G. *Int. J. Mass Spectrom.* **2007**, *265*, 237–243.
(83) Hadjar, O.; Futrell, J. H.; Laskin, J. *J. Phys. Chem. C* **2007**, *111*, 18220–18225.
(84) Fenn, J. B.; Mann, M.; Meng, C. K.; Wong, S. F.; Whitehouse, C. M. *Science* **1989**, *246*, 64–71.
(85) Laskin, J.; Denisov, E. V.; Shukla, A. K.; Barlow, S. E.; Futrell, J. H. *Anal. Chem.* **2002**, *74*, 3255–3261.

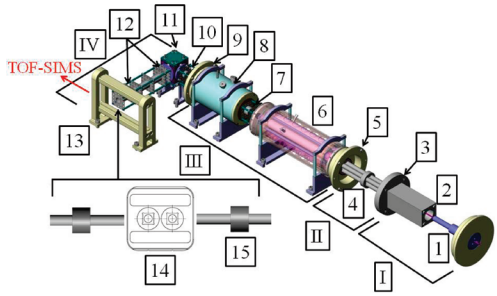

Figure 1. Schematic illustration of the ion deposition instrument: I, ion funnel region (7×10^{-1} Torr). II, collision quadrupole region (1×10^{-1} Torr). III, mass selection and focusing region (2×10^{-4} Torr). IV, deposition region (1×10^{-6} Torr). (1) heated capillary, (2) electrodynamic ion funnel, (3) first conductance limit, (4) first collision quadrupole, (5) second conductance limit, (6) resolving quadrupole, (7) 2 focusing lenses, (8) second collision quadrupole, (9) third conductance limit, (10) Einzel lens, (11) quadrupole bender, (12) two Einzel lenses, (13) target platform, (14) surface mount, (15) magnetic translators.

rates of between 20−50 μL/h are generally employed. The charged microdroplets emanating from the silica capillary are entrained in a gas flow and transferred from ambient pressure (760 Torr) into the first differentially pumped vacuum chamber (7×10^{-1} Torr) through a 16.5 cm long, 0.03 cm inner diameter heated (100−200 °C) stainless steel capillary biased at +300 V. The entrance of the stainless steel capillary is flared at 5° to a final internal diameter of 0.12 cm which provides a larger acceptance area and facilitates better overall transmission of ions from ambient pressure into vacuum.[86] The desolvated ions exiting the heated capillary are transferred into the second differentially pumped region (1×10^{-1} Torr) through an electrodynamic ion funnel of the design developed by Smith and co-workers.[87−89] The ion funnel is powered by a home-built high Q head and operated at a radio frequency (RF) of 400 kHz and a peak-to-peak RF amplitude of 70 V; the DC gradient along the ion funnel axis is created by biasing the front and back plates of the funnel to +300 and +50 V, respectively. A 1.5 mm inner diameter orifice in the back plate of the ion funnel serves as the conductance limit between the ion funnel and the first collision quadrupole region. Standard total ion currents of around 1 nA are obtained at this first conductance limit. The ion funnel region is differentially pumped to 7×10^{-1} Torr by an Adixen model 2063SD, 16 L/s pumping speed mechanical pump connected through a 5.08 cm inner diameter circular port (NW50) in the side of the vacuum chamber.

The first collision quadrupole (CQ1) is an RF only ion guide that serves to focus and thermalize the ions exiting the ion funnel before they are transferred into the mass resolving quadrupole. The CQ1 is constructed of four 15.0 cm long, 0.95 cm outer diameter stainless steel rods. The CQ1 is powered by an Ardara (Ardara Technologies, Ardara, PA) dual RF power supply operated at 1.4 MHz, a peak-to-peak RF amplitude of 350 V, and a DC bias of around +30 V. The CQ1 region is differentially pumped to a pressure of around 1×10^{-1} Torr by a Leybold D25B 10 L/s pumping speed mechanical pump through a 4 cm inner diameter port (NW40). A 0.2 cm inner diameter aperture biased at around +25 V limits the conductance between the collision quadrupole region and the following chamber which houses the mass resolving quadrupole. Typical total ion currents of 500 pA are obtained at this second conductance limit.

After exiting the first collision quadrupole the ions are mass selected by an Extrel (Extrel CMS, Pittsburgh, PA) Tri-Filter quadrupole mass filter with 19 mm diameter rods that is controlled by a 300 W, 880 kHz, QC-150 power supply. The RQ has a significantly larger inscribed diameter than a standard quadrupole with 9.5 mm diameter rods and provides a much wider acceptance area for ions exiting the first collision quadrupole region. The RQ has a mass range of up to 1000 amu for singly charged ions. A set of entrance and exit lenses, biased at approximately +30 V and +15 V, respectively, combined with RF pre- and post filters enable efficient transmission of mass-selected ions through the resolving quadrupole which is DC biased at around +20 V. Because of the large inscribed diameter (16.6 mm) of the resolving quadrupole, collisional focusing of the broad beam exiting the RQ in the following stage of the instrument is essential for efficient transmission of ions following mass selection.

Ions exiting the RQ are extracted by one 1.4 cm inner diameter tube lens biased at around −150 V and focused by a second tube lens, biased at roughly +15 V, into a second collision quadrupole housed inside a 7.5 cm outer diameter stainless steel collision cell. The second collision quadrupole (CQ2) is constructed from four 12.7 cm long, 0.95 cm outer diameter stainless steel rods. The CQ2 is powered by an Ardara dual channel RF power supply operated at 1.3 MHz, a peak-to-peak RF amplitude of 300 V, and a DC bias of around +10 V. A 3 mm inner diameter aperture, biased at approximately −10 V, serves as the conductance limit at the entrance of the collision cell, while a 2 mm inner diameter orifice, which is biased at roughly −5 V, limits conductance at the exit of the collision cell. A pressure of 1.6×10^{-3} Torr of Ar is maintained inside the collision cell using a low-flow leak valve to ensure efficient focusing of the ions through the 1.5 mm inner diameter aperture that separates the mass selection and focusing region from the final ion deposition region. This conductance limit is typically biased at a large attractive potential of −100 V for positive ions. The mass-selected ion currents obtained at this final conductance limit depend strongly on the relative yield of the selected ion in the overall ion distribution and how well the electrospray conditions are optimized to enhance that yield. Typical currents of between 50 and 150 pA are obtained for the doubly charged peptides and organometallic complexes reported in this study. The mass selection region is differentially pumped to 2×10^{-4} Torr by a Varian TV-301 Navigator 280 L/s pumping speed Turbo pump connected through a 10.16 cm inner diameter port (ISO 100). The turbo pump is backed by a Varian DS 302 5 L/s pumping speed mechanical pump.

After being focused in the second collision quadrupole, the ions are transmitted into the final deposition region. A set of two 1.4 cm inner diameter tubes and one 0.75 cm inner diameter plate

(86) Wu, S.; Zhang, K.; Kaiser, N. K.; Bruce, J. E. *J. Am. Soc. Mass Spectrom.* **2006**, *17*, 772–779.
(87) Shaffer, S. A.; Prior, D. C.; Anderson, G. A.; Udseth, H. R.; Smith, R. D. *Anal. Chem.* **1998**, *70*, 4111–4119.
(88) Shaffer, S. A.; Tolmachev, A.; Prior, D. C.; Anderson, G. A.; Udseth, H. R.; Smith, R. D. *Anal. Chem.* **1999**, *71*, 2957–2964.
(89) Kim, T.; Tolmachev, A. V.; Harkewicz, R.; Prior, D. C.; Anderson, G.; Udseth, H. R.; Smith, R. D.; Bailey, T. H.; Rakov, S.; Futrell, J. H. *Anal. Chem.* **2000**, *72*, 2247–2255.

serve as an Einzel lens that focuses the ions into an Ardara quadrupole bender (Ardara Technologies, Ardara, PA) that turns the ion beam 90° to prevent neutral molecules from impinging on the surface of the deposition target. The central tube of the Einzel lens is biased at −15 V and the entrance and exit optics are maintained at −100 V. The quadrupole bender is constructed from four 4 cm long, 1.5 cm radius rod quarters. The bender is capped on the top and bottom by two stainless steel plates and contains both an entrance and exit lens with a 0.75 cm inner diameter orifice. The potentials applied to the bender rods vary depending on the mass and energy of the mass-selected ions but are typically set in the range of −300 to 0 V. Following the bender, a series of two Einzel lenses, constructed from five 1.4 cm inner diameter tubes and one 0.75 cm inner diameter plate are employed to focus the ion beam to a final diameter of approximately 2−3 mm. Potentials of −30 and −10 V are applied to the central tubes of the first and second Einzel lenses, respectively, while the entrance and exit optics are maintained at −100 V. Typical mass-selected ion currents of between 50 and 100 pA are obtained at the surface for peptides and organometallic complexes. The final deposition region is differentially pumped to 1×10^{-6} Torr by a Varian TV-301 Navigator 280 L/s turbo pump connected through a 10.16 cm inner diameter port (ISO100). The turbo pump is backed by a Varian DS 302 5 L/s pumping speed mechanical pump.

Reactive Gas Exposure. The final deposition chamber is configured to allow the surfaces prepared or modified through ion soft and reactive landing to be exposed to controlled pressures of reactant gases. A 4.06 cm inner diameter port (NW40) has been machined in the lid of the chamber directly over the sample platform. A 6 way NW40 cross is installed at this port that accommodates one Varian (Varian Inc., Palo Alto, CA) MBA100 pressure gauge, two NorCal (Nor Cal Inc., Yreka, CA) high vacuum leak valves, and an Extorr XT100 (Extorr Inc., Kensington, PA) residual gas analyzer. The leak valves may each be connected to a separate gas cylinder to allow controlled partial pressures of two different reactant gases to be introduced into the deposition region. To facilitate better control over the total pressure in the chamber and to minimize the load on the turbo pump a 10.16 cm inner diameter (ISO100) gate valve is installed between the deposition chamber and the turbo pump. The residual gas analyzer consists of an electron impact ionizer coupled to a quadrupole mass analyzer and allows accurate measurement of reactant and product partial pressures up to a maximum mass of 100 amu.

Surface Interface. The mass-selected ion beam, which is focused to a final diameter of 3 mm, impinges at an angle of 90° onto a surface mounted in a custom designed sample holder compatible with the commercial TOF-SIMS analysis instrument described below. The sample holder is constructed from stainless steel and is 6.67 cm long, 1.5 cm thick, and 5.6 cm tall. The current design allows two 1 cm × 1 cm square target surfaces to be mounted side by side from the rear of the sample holder with the deposition surface facing the incoming ion beam. The targets are held in place by circular copper springs which are inserted behind the surfaces and expand outward forming a tight fit inside the circular cutouts in the sample holder. Rectangular cutouts above and below the square targets enable the surfaces, once mounted in the sample holder, to be carefully aligned with respect to the ion beam. Tapped holes at both ends allow two magnetic translators to screw into either side of the sample holder. A rail is machined into both the top and bottom of the sample holder to enable it to slide smoothly into the target platform in front of the ion beam. The target platform consists of two aluminum rails on the top and bottom held in place by a poly ether ether ketone (PEEK) mounting bracket on either end. The PEEK mounting brackets electrically isolate the sample holder from the vacuum chamber so that the surface may be floated and the incoming ion current measured using an electrometer (Keithley Instruments, Cleveland, OH).

The deposition chamber is connected through a 12.7 cm long, 7.62 cm outer diameter (ISO80) tube fitting to the commercial TOF-SIMS analysis instrument. To enable independent operation and maintenance of both the deposition and analysis instruments a 7.62 cm (ISO80) inner diameter gate valve is installed between the two machines. The deposition surface is introduced into vacuum through a load-lock chamber on the TOF-SIMS instrument. The sample holder is lowered into the load-lock chamber and threaded onto the end of the first magnetic manipulator. After the load-lock chamber is pumped out, the gate valve separating this region from the SIMS analysis chamber is opened and the first magnetic manipulator is used to move the sample holder from the load-lock region onto the SIMS analysis stage which is mounted on an x-y translator driven by stepper motors. The SIMS analysis chamber is pumped to a pressure 4×10^{-10} Torr. Once the sample holder is firmly engaged with the SIMS analysis stage the first magnetic manipulator is unthreaded and retracted back into the load-lock region and the gate valve separating the two regions is closed. A SIMS analysis may then be conducted on the surface prior to ion soft landing to establish a background mass spectrum. Once the background spectrum is acquired, the x-y translation stage is moved toward the deposition chamber. The gate valve between the deposition apparatus and SIMS instrument is opened and a second magnetic manipulator arm is brought into the SIMS analysis chamber, threaded into the sample holder, and used to move the sample holder from the SIMS analysis chamber onto the sample platform housed within the deposition chamber. In order to measure the ion current impinging on the surface during deposition it is necessary that the second magnetic manipulator, which is electrically connected to the vacuum chamber, be disengaged from the sample holder and retracted. After the completion of soft or reactive landing the second manipulator is threaded back into the sample holder and used to transfer the surface into the SIMS analysis chamber.

TOF-SIMS Analysis. Surfaces generated or modified through soft and reactive landing are analyzed in situ using a PHI TRIFT II TOF-SIMS instrument (Physical Electronics, Eden Prairie, MN). In TOF-SIMS the sample is bombarded by 15 keV primary gallium ions (Ga^+, 500 pA, 5 ns pulse width, 10 kHz repetition rate) which induces desorption of material from the surface.[90] The secondary ions ejected from the surface are extracted into the mass analyzer which consists of three separate electrostatic sectors. The mass spectrometer compensates for any energy dispersion of the secondary ions and achieves a mass resolution

(90) Wucher, A. *Appl. Surf. Sci.* **2006**, *252*, 6482–6489.

of around 4000 at 1000 amu. All spectra were acquired for 2 min using a 15 keV Ga^+ primary ion beam.

Chemicals and Materials. The gold substrates used to create alkyl thiol self-assembled monolayers were purchased from Platypus Technologies (Madison, WI) and have the following specifications: 10×10 mm^2, 525 um thick Si, 50 Å Ti adhesion layer, 1000 Å Au layer. 1H, 1H, 2H, 2H - Perfluorodecanethiol and 16-Mercaptohexadecanoic acid were purchased from Sigma (Sigma-Aldrich, St. Louis, MO) and Asemblon (Asemblon Inc., Redmond, WA), respectively. The FSAM and COOH-SAM surfaces were prepared following literature procedures[91,92] with the substitution of HPLC grade methanol as the solvent which was purchased from Fisher (Fisher Scientific, Pittsburgh, PA). The acetic acid used for the preparation of the COOH-SAM was also purchased from Fisher. The gold substrates were cleaned using a Boekel (Boekel Scientific, Feasterville, PA) ultraviolet cleaner and immersed in glass scintillation vials containing 1 mM solutions of thiol in methanol. The monolayers were allowed to assemble for at least 12 h and then ultrasonically washed for 5 min in methanol for FSAMs and a methanol acetic acid solution for COOH-SAMs. The surfaces were then rinsed with pure methanol, dried with N_2 and mounted in the SIMS sample holder. Gramicidin S and tris(2,2′-bipyridyl)dichlororuthenium(II) hexahydrate were both purchased from Sigma-Aldrich. The powder solids were dissolved in methanol to create stock solutions with a concentration of 1×10^{-3} M. The stock solutions were diluted by either a factor of 10 or 100 to achieve optimum electrospray ionization.

RESULTS AND DISCUSSION

Mass-Selected Deposition of Gramicidin onto FSAM Surfaces. To enable a comparison between in situ analysis by TOF-SIMS and FTICR-SIMS, doubly protonated Gramicidin S, $[GS + 2H]^{2+}$, was soft-landed onto an FSAM surface. Both singly and doubly protonated GS were produced through electrospray ionization of a 1×10^{-5} to 1×10^{-4} M solution in methanol. A mass-selected ion current of 85 pA of $[GS + 2H]^{2+}$ was directed at the center of the 10×10 mm surface for 70 min corresponding to a total delivery of 1.1×10^{12} ions. A potential of +20.5 V was applied to the second collision quadrupole and the sample platform was at ground potential. The distribution of ion kinetic energies at the surface, measured using a retarding potential analysis, is plotted in Figure 2. The distribution is bimodal and is peaked at slightly under 20 V with a smaller peak at slightly lower energy. The bimodal distribution of ion energies results from collisions between the mass-selected ions extracted from the second collision quadrupole and the Ar gas escaping through the exit aperture of CQ2. Figure 3a shows the TOF-SIMS spectrum obtained 5 min after the end of deposition. Figure 3b presents the FTICR-SIMS spectrum obtained previously[83] after 58 min of soft landing of 16 pA of $[GS + 2H]^{2+}$ corresponding to a total ion delivery of 1.8×10^{11} ions. Close inspection of the mass range between 0 and 1500 amu reveals a few similarities and some striking differences between the two spectra. Both in situ

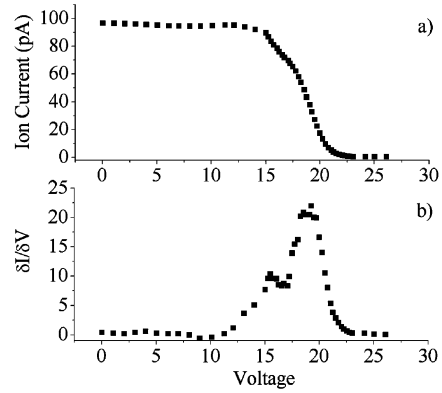

Figure 2. Plot of (a) measured ion current (pA) and (b) dI/dV vs retarding potential (V) for $[GS + 2H]^{2+}$ ($m/z = 571.4$) with DC bias of second collision quadrupole set to +20.5 V.

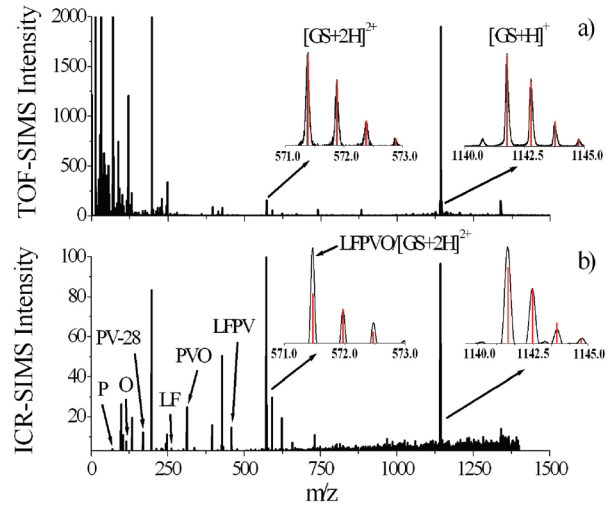

Figure 3. (a) TOF-SIMS and (b) FTICR-SIMS spectra (m/z = 0−1500) obtained after mass-selected deposition of $[GS + 2H]^{2+}$ (m/z = 571.4) onto FSAM.

SIMS techniques produce peaks characteristic of the mass-selected doubly protonated ion $[GS + 2H]^{2+}$ ($m/z = 571.4$) and the singly protonated ion $[GS + H]^+$ ($m/z = 1141.7$). However, in the case of the FTICR-SIMS spectra, the relative intensities of the peaks at $m/z = 571.4$ and 1141.7 are similar while in the TOF-SIMS spectra, the peak corresponding to the singly charged ion is far more intense than the peak for the doubly charged species. Closer examination of the $[GS + 2H]^{2+}$ peak in the mass range of 571 − 573 amu reveals that the isotopic pattern of the $[GS + 2H]^{2+}$ peak in the TOF-SIMS spectrum matches, almost perfectly, the simulated pattern calculated using the molecular weight calculator program (http://omics.pnl.gov/software/MWCalculator.php). In comparison, the distribution of peak intensities in this mass range in the FTICR-SIMS spectrum does not match the calculated isotopic pattern due to an enhanced abundance of the leading peak at 571.4 amu. The higher intensity of this peak in the FTICR-SIMS spectrum results from the mass overlap between $[GS + 2H]^{2+}$ and the singly charged fragment ion LFPVO (m/z = 571.4).[83] In comparison, the peaks obtained for singly protonated $[GS + H]^+$ by both TOF and FTICR-SIMS match the simulated spectra very well. These findings demonstrate

(91) Chidsey, C. E. D.; Liu, G. Y.; Rowntree, P.; Scoles, G. *J. Chem. Phys.* **1989**, *91*, 4421–4423.
(92) Wang, H.; Chen, S. F.; Li, L. Y.; Jiang, S. Y. *Langmuir* **2005**, *21*, 2633–2636.

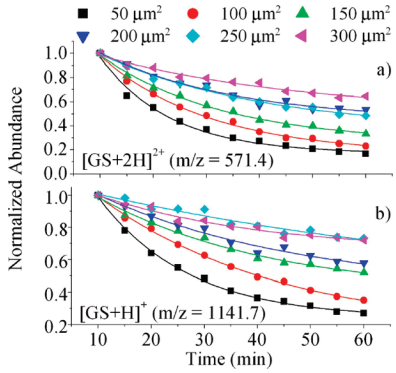

Figure 4. Kinetic plots obtained for (a) $[GS + 2H]^{2+}$ ($m/z = 571.4$) and (b) $[GS + H]^{+}$ ($m/z = 1141.7$) following deposition of $[GS + 2H]^{2+}$ onto FSAM.

the ability of both SIMS techniques to resolve $[GS + 2H]^{2+}$ from LFPVO and indicate that analysis by FTICR-SIMS results in production of the LFPVO fragment which is not observed with TOF-SIMS. In addition to the abundant LFVPO peak, the FTICR-SIMS spectrum contains a number of other peptide related fragments LFPV ($m/z = 457.3$), FPVO-NH_3 ($m/z = 441.3$), LFPV-28 ($m/z = 438.3$), PVO ($m/z = 311.2$), LF ($m/z = 261.2$), LF-28 ($m/z = 233.2$) and PV-28 ($m/z = 169.1$), and immonium ions of proline (P) ($m/z = 70.07$) and ornithine (O) ($m/z = 115.09$).[83] In comparison, the TOF-SIMS spectrum is differentiated by much less fragmentation with pronounced fragment peaks appearing only for PV-28 ($m/z = 169.1$), P ($m/z = 70.07$) and O ($m/z = 115.09$). The differences in fragmentation behavior observed in the spectra obtained by TOF and FTICR-SIMS can be attributed to the variation in time between sputtering of the surface with the primary ions and mass analysis of the ejected secondary ions. During FTICR-SIMS analysis, the time between the sputtering event and the excitation/detection step is on the order of a few milliseconds.[31] The TOF-SIMS analysis, in comparison, is much faster with only a few microseconds between the sputtering event and detection. Due to the significantly longer residence time of the energized secondary ions prior to analysis in FTICR-SIMS there is a much higher incidence of unimolecular decay and fragmentation as compared to TOF-SIMS.[39,93,94] The lower fragmentation yield observed in TOF-SIMS spectra is advantageous for the interpretation of SIMS spectra and for improved detection of secondary ions because signal intensity is distributed over fewer peaks.

The utility of in situ TOF-SIMS characterization for studying charge reduction and desorption kinetics was explored by examining the evolution of the TOF-SIMS spectrum of $[GS + 2H]^{2+}$ softlanded onto FSAM. In these experiments TOF-SIMS spectra were acquired for 1 min every 5 min for a total of 60 min following the end of soft landing. Both the doubly and singly protonated peaks exhibited exponential decays in intensity with respect to time as shown in Figure 4a for $[GS + 2H]^{2+}$ ($m/z = 571.4$) and Figure 4b for $[GS + H]^{+}$ ($m/z = 1141.7$). Close inspection of Figure 4 reveals that the decay rate for the doubly protonated peptide is consistently higher than for the singly protonated species. These results differ somewhat from the

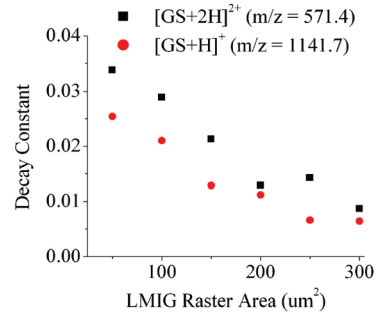

Figure 5. Plot of exponential decay constant vs LMIG raster area (μm) for $[GS + 2H]^{2+}$ ($m/z = 571.4$) and $[GS + H]^{+}$ ($m/z = 1141.7$) following deposition of $[GS + 2H]^{2+}$ onto FSAM.

behavior observed previously for $[GS + 2H]^{2+}$ deposited onto FSAM and monitored by FTICR-SIMS.[83] In the prior study, the intensity of $[GS + 2H]^{2+}$ was found to decay exponentially with time while $[GS + H]^{+}$ exhibited an initial increase in intensity followed by a stable plateau that lasted for several hours. The different charge reduction behavior observed for the two in situ SIMS techniques suggests that the TOF-SIMS analysis perturbs the sample in a way that FTICR-SIMS does not. The FTICR-SIMS analysis employs 8 keV Cs^+ primary ions (4 nA, 80 μs pulse width, 4.6 mm spot diameter) corresponding to a total ion flux of 10^{10} ions/cm^2.[83] In comparison, the TOF-SIMS technique uses 15 keV Ga^+ ions (500 pA, 5 ns pulse width, 100 μm^2 area) corresponding to a higher primary ion flux of 10^{11} ions/cm^2.[32] To test whether the higher primary Ga^+ ion flux influences the charge reduction and desorption kinetics, a series of six separate soft landing experiments were conducted where 1.1×10^{12} ions of $[GS + 2H]^{2+}$ were deposited onto FSAM surfaces. A separate TOF-SIMS analysis was conducted for each deposition employing a different Ga^+ raster area. The Ga^+ raster area defines the area that is sputtered by the primary Ga^+ ions during analysis. By maintaining a constant ion current (500 pA) and increasing the raster area from 50 μm^2 to 300 μm^2 we were able to examine the influence of the primary ion flux on the observed charge reduction and desorption kinetics. Inspection of Figure 4 reveals that as the raster area is increased, and thereby, the primary ion flux decreased, the rate of decay of both $[GS + 2H]^{2+}$ and $[GS + H]^{+}$ decreases. The decreasing trend in the rate of exponential decay as a function of raster area is plotted in Figure 5. These results strongly indicate that higher Ga^+ primary ion fluxes during TOF-SIMS analysis accelerate the rate of charge neutralization and desorption of positively charged ions on inert FSAMs. This is a somewhat surprising finding as the ion dose of 10^{11} ions/cm^2 at a raster area of 100 μm^2 is well below the static limit at which ablation of the SAM surface has been estimated to occur ($10^{12} - 10^{13}$ ions/cm^2).[95] Based on literature values for the packing of FSAM molecules on gold,[96] it is estimated that there are approximately 5×10^6 thiol molecules per square μm on the surface. Assuming a total soft-landed ion delivery of 1×10^{12} ions to a circular spot 3 mm in diameter, there are roughly 1×10^5 ions/μm^2. Therefore, because the soft-landed ions are not as dense as the FSAM monolayer,

(93) Rakov, V. S.; Futrell, J. H. *Eur. J. Mass Spectrom.* **2002**, *8*, 253–262.
(94) Pachuta, S. J.; Cooks, R. G. *Chem Rev* **1987**, *87*, 647–669.
(95) Benningh., A. *Z. Phys.* **1970**, *230*, 403–417.
(96) Pflaum, J.; Bracco, G.; Schreiber, F.; Colorado, R.; Shmakova, O. E.; Lee, T. R.; Scoles, G.; Kahn, A. *Surf. Sci.* **2002**, *498*, 89–104.

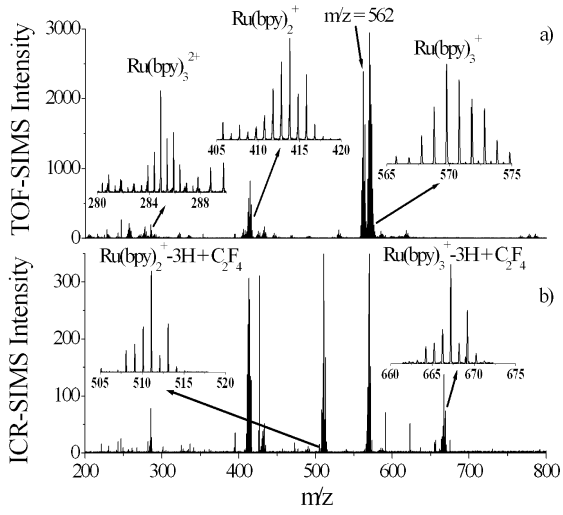

Figure 6. (a) TOF-SIMS and (b) FTICR-SIMS spectra (m/z = 200 − 800) obtained after mass-selected deposition of $Ru(bpy)_3^{2+}$ (m/z = 285.06) onto FSAM.

the TOF-SIMS analysis is in the static SIMS regime for the monolayer but not for the deposited material. Indeed, as the raster area is increased from 50 μm^2 to 300 μm^2 the population of deposited ions sampled by the Ga^+ sputtering increases from 7×10^6 to 4×10^7 ions. This increase in population of ions may also explain the reduction in the rate of charge neutralization and desorption of the soft-landed species with increasing raster area. Moreover, in a previous publication[81] it was estimated that positively charged ions interacting with an FSAM surface ($\alpha = 6.8 \times 10^{-24}$ cm^3) have a physisorption energy of roughly 20 kcal/mol. It appears that in this range of binding energies it is crucial to carefully select the primary ion beam flux when studying the kinetics of desorption and neutralization processes. Furthermore, these findings indicate that there is an advantage to using FTICR-SIMS instead of TOF-SIMS for such kinetic studies because FTICR-SIMS samples a larger area of the surface with the primary ions. In the following sections we present examples of experiments for which the advantages of analysis by TOF-SIMS over FTICR-SIMS is obvious.

Mass-Selected Deposition of $Ru(bpy)_3^{2+}$. The ultimate intended application of the ion deposition apparatus described herein is to prepare catalytic surfaces through the soft and reactive landing of clusters and organometallic complexes and to react and analyze them using in situ TOF-SIMS. As a first test of the capabilities of the apparatus for this application we soft-landed ruthenium tris-bipyridine ($Ru(bpy)_3^{2+}$) dications onto FSAM surfaces. This complex was selected due to widespread interest in its application as a photosensitizer for water oxidation catalysis.[97,98] During the experiment, an ion current of 50 pA of mass selected $Ru(bpy)_3^{2+}$ was directed at the surface for 2 h corresponding to a total ion exposure of 1.1×10^{12} ions. Figure 6a presents the TOF-SIMS spectrum (m/z = 200 − 800) obtained 5 min after the end of soft landing. To facilitate another comparison between in situ analysis by TOF and FTICR-SIMS, we also conducted a deposition and analysis using the instrument described previously.[31] Figure 6b shows the spectrum obtained by FTICR-SIMS after soft landing of 50 pA of $Ru(bpy)_3^{2+}$ for 1 h corresponding to a total ion exposure of 5.6×10^{11} ions. Both spectra in Figure 6 exhibit strong peaks characteristic of the doubly charged $Ru(bpy)_3^{2+}$ (m/z = 285.06) as well as the singly charged $Ru(bpy)_3^+$ (m/z = 570.11). In addition, a strong peak at m/z = 414.04 corresponding to the doubly ligated $Ru(bpy)_2^+$ ion is observed in both spectra. Both in situ techniques, therefore, indicate that a fraction of doubly charged $Ru(bpy)_3^{2+}$ is converted rapidly to singly charged $Ru(bpy)_3^+$ following soft landing onto FSAM surfaces. This is consistent with previous results from our laboratory which have shown instantaneous loss of charge through electron transfer from gold to deposited ions at defect sites in monolayers.[99] The kinetics of charge neutralization of permanent (unprotonated) ions deposited onto various SAMs will be the subject of a forthcoming publication. In addition to charge reduction, it is shown that a significant portion of the triply ligated species fragments by losing one bipyridine ligand during SIMS analysis and that the intensity of this fragment is relatively higher in the FTICR-SIMS spectra compared to the TOF-SIMS results. Close inspection of Figure 6 reveals that there are also additional peaks in the FTICR-SIMS spectrum that do not appear in the TOF-SIMS analysis. The most pronounced of these is the peak at m/z = 511.04 which corresponds to $[Ru(bpy)_2\text{-}3H + C_2F_4]^+$. A similar species is also observed at m/z = 667.1 which is identified as $[Ru(bpy)_3\text{-}3H + C_2F_4]^+$. Both of these products likely result from the interaction of highly energized fragments in the plume of secondary ions emitted from the surface during sputtering. This process is more pronounced in FTICR-SIMS because of a longer delay time (milliseconds) between the sputtering and analysis as compared to TOF-SIMS (microseconds). The presence of such products in FTICR SIMS spectra is detrimental both for the spectral quality and interpretation.

There is also one prominent peak present in the TOF-SIMS spectrum that is absent in the FTICR-SIMS analysis. This peak, which has an isotopic distribution consistent with ruthenium, is located at m/z = 562.5 and exhibits growth in relative intensity with time suggesting that it results from reaction between the deposited $Ru(bpy)_3^{2+}$ ions and an unknown impurity in the FSAM surface. TOF-SIMS spectra of FSAM surfaces prepared in our laboratory using different solvents have shown that the number and relative intensity of impurity peaks vary strongly depending on the solvent used. In the FTICR-SIMS studies we used nondenatured 200 proof ethanol as the solvent for alkyl thiols but switched recently to methanol for the TOF-SIMS experiments due to high intensity contaminants from the ethanol at m/z = 325. When methanol was used as the solvent, the TOF-SIMS background spectrum obtained prior to ion deposition was much cleaner than with ethanol. Recent studies, however, have shown that both commercial HPLC and RPE grade methanol contain organic impurities that can lead to the formation of larger hydrocarbon species.[100] While we cannot give a definitive chemical assignment at this time, we propose

(97) Concepcion, J. J.; Jurss, J. W.; Brennaman, M. K.; Hoertz, P. G.; Patrocinio, A. O. T.; Iha, N. Y. M.; Templeton, J. L.; Meyer, T. J. *Acc. Chem. Res.* **2009**, *42*, 1954–1965.
(98) Duan, L. L.; Xu, Y. H.; Zhang, P.; Wang, M.; Sun, L. C. *Inorg. Chem.* **2010**, *49*, 209–215.
(99) Laskin, J.; Wang, P.; Hadjar, O. *J. Phys. Chem. C* **2010**, *114*, 5305–5311.
(100) Guella, G.; Ascenzi, D.; Franceschi, P.; Tosi, P. *Rapid Commun. Mass Spectrom.* **2007**, *21*, 3337–3344.

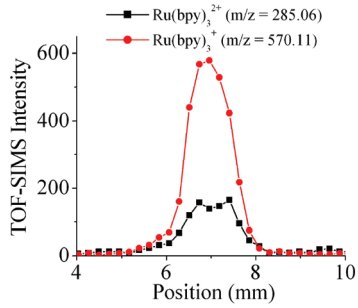

Figure 7. TOF-SIMS line profile of the deposited spot plotted as the integral peak signal of $Ru(bpy)_3^{2+}$ ($m/z = 285.06$) and $Ru(bpy)_2^{+}$ ($m/z = 570.11$) on the COOH-SAM surface along the *x*-axis.

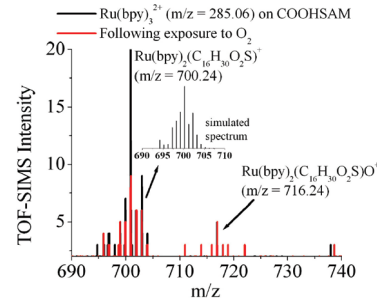

Figure 8. TOF-SIMS spectra ($m/z = 690 - 740$) following deposition of $Ru(bpy)_3^{2+}$ ($m/z = 285.06$) onto COOH-SAM surface and following exposure to 1×10^{-4} Torr of O_2. Note the peaks around $m/z = 700$ corresponding to $Ru(bpy)_2(C_{16}H_{30}O_2S)^+$ and $Ru(bpy)_2(C_{16}H_{30}O_2S)O^+$.

that the peak at $m/z = 562.5$ corresponds to $Ru(bpy)_2C_6H_{12}O_4^+$ and results from reaction with residual impurities in the monolayer. With the exception of this mystery peak, the results for the soft landing of $Ru(bpy)_3^{2+}$, therefore, are qualitatively similar to the results for deposition of $[GS + 2H]^{2+}$ onto FSAM. Both systems are characterized by a higher incidence of fragmentation and ion−molecule reaction products when analyzed by FTICR-SIMS than by TOF-SIMS. It follows that TOF-SIMS analysis greatly simplifies the identification of sputtered ions.

One of the undesirable aspects of using homogeneous, solution-phase catalysts to promote reactions is the unavoidable final step of separating the products from the catalyst.[61] Through immobilization of molecular catalysts on inorganic substrates it is possible to retain or enhance the activity of the metal center while making separation of the catalyst from the products much easier.[62] In this manner, the surface acts as a "rigid ligand" that holds the complex in place.[60] Self-assembled monolayers, which have some degree of physical flexibility and may be terminated with various functional groups, appear as promising templates to study the immobilization of organometallic complexes on surfaces through ion deposition. To examine the feasibility of tethering metal complexes to surfaces through reactive landing we deposited $Ru(bpy)_3^{2+}$ onto a carboxylic acid terminated COOH-SAM. During the experiment, 55 pA of mass selected $Ru(bpy)_3^{2+}$ was directed at the COOH-SAM surface for 155 min corresponding to a total ion exposure of 1.5×10^{12} ions. The TOF-SIMS *x*-axis line profile of the deposited spot plotted as the integral peak signal of $Ru(bpy)_3^{2+}$ ($m/z = 285.06$) and $Ru(bpy)_3^{+}$ ($m/z = 570.11$) is shown in Figure 7. The spot has a diameter of approximately 2 mm and is characterized by a significantly higher yield of the singly charged $Ru(bpy)_3^{+}$ species. The less intense doubly charged $Ru(bpy)_3^{2+}$ ion exhibits a small drop in intensity at the center of the spot. The overall mass spectrum between $m/z = 200$ and 800 is qualitatively similar to that shown in Figure 6a for the deposition of $Ru(bpy)_3^{2+}$ onto FSAM. One striking difference, however, is observed in the mass range between $m/z = 690$ and 740. As shown in Figure 8, there is an appreciable intensity of a peak centered at $m/z = 700.24$, which is characteristic of a $Ru(bpy)_2$ complex bound to one intact thiol molecule ($C_{16}H_{30}O_2S$). Comparison to the simulated spectrum obtained using the molecular weight calculator program reveals close agreement for a species with the formula $Ru(bpy)_2(C_{16}H_{30}O_2S)^+$. This result suggests that reactive landing of $Ru(bpy)_3^{2+}$ onto COOH terminated SAMs results in the loss of one bipyridine ligand from the complex accompanied by attachment of one intact thiol molecule. Carboxylic acid groups are known to interact with metals to form a salt and hydrogen according to eq 1.

$$CH_3COOH + M \rightarrow CH_3COOM + H \qquad (1)$$

Such a reaction between $Ru(bpy)_3^{2+}$ and the COOH-SAM to form a strongly bound complex is consistent with the observation of the $Ru(bpy)_2(C_{16}H_{30}O_2S)^+$ peak in the TOF-SIMS spectrum and suggests strong immobilization of the metal complex on the thiol surface. To test the reactivity of the immobilized complex we exposed the surface to 1×10^{-4} Torr of O_2 for 20 min by leaking a controlled flow of gas into the deposition chamber. Following exposure to O_2 the deposition chamber was pumped out and the sample was transferred back into the TOF-SIMS analysis chamber (4×10^{-10} Torr). The spectrum obtained after O_2 exposure shows a reduction in the relative intensity of $Ru(bpy)_2(C_{16}H_{30}O_2)^+$ and a concomitant increase in intensity at $m/z = 716.24$. This peak likely corresponds to the association of one oxygen atom onto the thiol bound ruthenium complex to form $Ru(bpy)_2(C_{16}H_{30}O_2)O^+$. This result suggests that organometallic complexes may be immobilized onto self-assembled monolayer surfaces through reactive landing and that the resulting surface exhibits reactivity toward a common oxidant. We can exclude reaction between oxygen and the alkyl thiol because the SAM surface is exposed to atmospheric oxygen during preparation of the monolayer and transfer of the substrate from solution into vacuum. The addition of oxygen to the immobilized complex is observed only after a controlled exposure of the substrate to O_2 in vacuum. Additional proof of strong immobilization was obtained by examining an *x*-axis line profile taken after exposure to O_2 which showed no broadening of the peak and, therefore, no migration or diffusion of the Ru complexes on the surface. Comparison of these results with the spectra obtained previously for the same deposition using FTICR-SIMS demonstrates the greater dynamic range and higher overall sensitivity of the TOF-SIMS technique. In the previous FTICR-SIMS spectra, the thiol adduct was barely observed at noise level. In comparison, TOF-SIMS achieves facile detection of this low abundance species and enables its reactivity with gaseous reagents to be studied.

CONCLUSION

Soft and reactive landing of mass-selected ions onto surfaces has a variety of potential applications in biological screening, materials science and catalysis. Through controlled deposition of small clusters and organometallic complexes onto chosen supports it is possible to generate monodisperse materials with enhanced catalytic activity toward desirable reactions. However, for preparative mass spectrometry to make the transition from a tool in the fundamental sciences to a practical approach for the fabrication of materials, it is crucial to understand the factors influencing the efficiency of soft and reactive landing and the robustness of the resulting materials. Characterization of surfaces produced or modified by ion deposition is, therefore, a critical step in the further development of this promising approach to nanoscale engineering.

In this publication, we describe the design and application of a new apparatus that enables in situ reactivity testing and TOF-SIMS analysis of materials created or modified through the deposition of mass-selected ions onto surfaces. The instrument employs a high transmission electrospray ionization source, two collision quadrupoles, a mass resolving quadrupole filter, and a 90° quadrupole bender that prevents neutral contaminants from impinging on the deposition surface. Currents of 50−100 pA of mass-selected ions focused onto a 2−3 mm diameter spot are routinely obtained at the surface for peptides and organometallic complexes. The kinetic energy of the ions impacting the surface is controlled by varying the potentials applied to the second collision quadrupole and the surface. The in situ TOF-SIMS analysis technique was validated through comparison to results obtained previously by in situ FTICR-SIMS. The results for the soft landing of $[GS + 2H]^{2+}$ onto FSAM surfaces demonstrate that the TOF-SIMS technique is characterized by less fragmentation and higher sensitivity than FTICR-SIMS. The flux of the primary Ga^+ ions is shown to exhibit a pronounced influence on the charge reduction and desorption kinetics of GS observed using TOF-SIMS emphasizing that care must be taken to ensure that the analysis is conducted in the static SIMS regime for the deposited material. As a first test of the capability of the apparatus to immobilize organometallic complexes on surfaces, the soft and reactive landing of $Ru(bpy)_3^{2+}$ onto both FSAM and COOH-SAM surfaces was examined. Comparison of the TOF-SIMS results for deposition onto FSAMs with the spectra obtained previously by FTICR-SIMS indicates a higher incidence of fragmentation and in-plume ion−molecule reactions in FTICR-SIMS analysis. High dynamic range of the TOF-SIMS enables detection of low-abundance species produced by reactive landing of $Ru(bpy)_3^{2+}$ onto COOH-SAM surfaces. It is demonstrated that deposition results in strong immobilization of metal complexes, as evidenced by the presence of the $Ru(bpy)_2$ thiol complex in the TOF-SIMS spectrum. In contrast, this complex is only observed at the noise level in the FTICR SIMS spectrum. In addition, it is shown that the immobilized complexes, which consists of a $Ru(bpy)_2$ center bound to an intact thiol, exhibit reactivity toward gaseous O_2.

The initial results presented in this publication demonstrate that in situ reactivity testing combined with TOF-SIMS analysis constitutes a powerful approach for characterizing the fundamentals of catalyst preparation using mass-selected ion deposition. The wide dynamic range, high sensitivity, low fragmentation yield, and low yield of products of in-plume reactions are unique advantages of in situ TOF-SIMS analysis. The simpler spectra, where the ion intensity is distributed over fewer peaks, offer significant advantages over analysis by FTICR-SIMS. Coupled with mass-selected ion deposition, the in situ TOF-SIMS technique will be used to examine the feasibility of using functionalized alkyl thiols as templates for the immobilization of organometallic catalysts and small nanoparticles and clusters.

ACKNOWLEDGMENT

We acknowledge support for this research by a grant from the Chemical Sciences Division, Office of Basic Energy Sciences of the U.S. Department of Energy (DOE), and the Laboratory Directed Research and Development Program at the Pacific Northwest National Laboratory (PNNL). This work was performed at the W. R. Wiley Environmental Molecular Sciences Laboratory (EMSL), a national scientific user facility sponsored by the U.S. DOE of Biological and Environmental Research and located at PNNL. PNNL is operated by Battelle for the U.S. DOE. M.L. acknowledges support from the DOE Science Undergraduate Laboratory Internship (SULI) program at Pacific Northwest National Laboratory (PNNL). We also gratefully acknowledge the technical help of James Ewing, Mark Townsend, Michael Russcher, and Beverly Taylor (PNNL).

Received for review March 22, 2010. Accepted May 17, 2010.

AC100734G